Journal of Materials Chemistry A

Accepted Manuscript

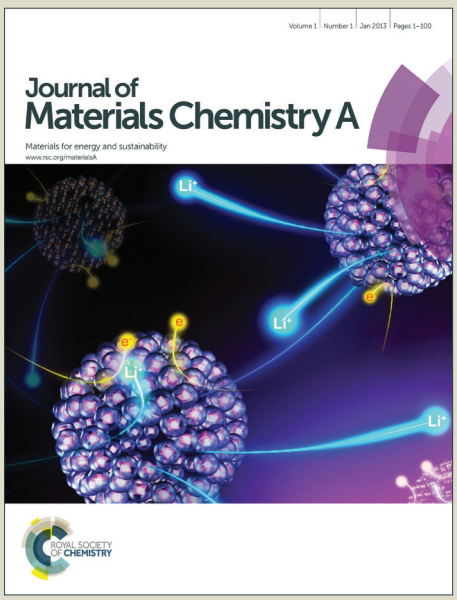

ROYAL SOCIETY OF CHEMISTRY

www.rsc.org/materialsA

Toc

A Conductive Liquid Crystal via Facile Doping of an n-Type Benzodifurandione Derivative

Bin Zhao[+,a,b], Chang-Zhi Li[+,a], Sheng-Qiang Liu[a], Jeffrey J. Richards[c], Chu-Chen Chueh[a], Feizhi Ding[d], Lilo D. Pozzo[c], Xiaosong Li[d], Alex K.-Y. Jen[*a,d]

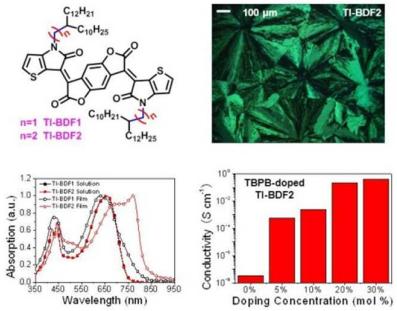

Liquid crystalline n-type molecular semiconductors exhibit interesting molecular order/charge-transport correlations, and allow n-doping with phosphonium salt to afford high conductivities.

Journal of Materials Chemistry A RSCPublishing

ARTICLE

A Conductive Liquid Crystal via Facile Doping of an n-Type Benzodifurandione Derivative

Cite this: DOI: 10.1039/x0xx00000x

Bin Zhao[+,a,b], Chang-Zhi Li[+,a], Sheng-Qiang Liu[a], Jeffrey J. Richards[c], Chu-Chen Chueh[a], Feizhi Ding[d], Lilo D. Pozzo[c], Xiaosong Li[d], Alex K.-Y. Jen[*a,d]

Received 00th December 2014,
Accepted 00th

DOI: 10.1039/x0xx00000x

www.rsc.org/

Two n-type molecular organic semiconductors (TI-BDF1 and TI-BDF2) consisting of thiophene-substituted indolin-2-one (TI) and benzodifurandione (BDF) with different branched side-chains have been synthesized to study the effect of molecular structure on molecular order, liquid crystal (LC) properties, and charge-transport. By tuning the branching point of the side-chains, TI-BDF2 shows a preferable edge-on π-face orientation and a high degree of liquid crystallinity, resulting in 4 orders of magnitude higher electron mobility than that of TI-BDF1. Subsequent n-doping of TI-BDF2 thin film with a thermally stable phosphonium salt affords a high electrical conductivity of 0.4 S cm^{-1}.

Introduction

Organic charge-transporting materials have drawn significant attention from researchers because of their potential for inexpensive, light-weight, flexible and scalable organic electronics.[1] To this end, solution processable organic semiconductors and conductors are ideal candidates for low-cost roll-to-roll fabrication. Although both p- and n-type semiconductors need to be significantly advanced as the complimentary pair of electronic components, the development of solution-processable n-type semiconductors and n-doped systems are lagging behind compared to their p-type counterparts.[2-4] There are only a limited library of building blocks that have been explored for n-type materials,[4] such as perylene diimide,[5] fullerene,[6] diketo-pyrrolopyrrole,[7, 8] benzodifurandione,[9] quinoidal thiophene,[8, 10] and isoindigo, etc.[11-12] Molecular engineering has often been performed to chemically modify electron-deficient aromatics into planar π-extended structures to promote intra- and inter-molecular π-wave function delocalization for improving their charge-transporting properties. In addition, side-chain engineering (i.e. modifying the length and branching point of alkyl chain) has also been used to optimize molecular ordering and stacking in thin film for efficient charge transport.[13-15]

By combining these two approaches, we have explored the feasibility of developing molecular liquid crystals (LCs) with extended π-planar structure as efficient n-type charge-transporting materials, because LCs can offer unique features of self-healing to repair structural defects and molecular alignments upon external treatments (i.e. annealing or shearing). Certain LCs with large mesogen centers are known to preserve their LC phase in a broad temperature window from room temperature to over 150 °C,[16-19] which are advantageous for obtaining ordered and stable LC phase for efficient charge transport. To date, only a few n-type semiconductors[20-23] show thermotropic LC behavior with one pure phase over the wide temperature ranges. Such LCs can provide interesting models for understanding how molecular structure affects LC phase order, and ultimately determines their charge-transporting properties.

In addition to improving molecular ordering in solids, the subsequent modulation of the carrier density of n-type organic solids by doping is another important yet hard-to-realize aspect for developing efficient solution-processable n-type conductors.[24-27] In general, strong chemical reducing agents (dopants) are used for n-doping, which tends to create unstable species under environmental conditions (oxygen and moisture). This creates significant obstacles for further development of solution processable n-doped organics. Recently, we have discovered that anion-induced electron transfer (AIET) process can be an effective mean to induce mild n-doping of semiconductors through selected anions of organic salts.[28] This is accomplished through either direct electron transfer or disassociation of anion-π charge transfer complex into charged species (in the case of mediating weak anions) dependent on the Lewis basicity of the corresponding anions.[28-31] Such mild doping does not need extra thermal or irradiative activation to enable fulleropyrrolidinium iodide (FPI) to reach conductivity as high as 0.03 Scm^{-1} and greatly enhanced environmental stability of organic electronics.[32] Therefore, it would be ideal if this approach can be applied to solution processable n-doped liquid crystal for electronic applications.

Herein, we report two novel n-type organic semiconductors, namely, TI-BDF1 and TI-BDF2 (**Scheme 1**), in which thiophene-substituted indolin-2-one (TI) moieties are condensed with benzodifurandione (BDF) to give coplanar molecules. It was found that a minimal change of their side-chains could dramatically alter the molecular order, thermal LC and charge-transporting properties of two molecules. With only a slight change of side-chain branch point, TI-BDF2 exhibits a superior liquid crystalline behavior and preferable edge-on π-face orientation towards the substrate, while TI-BDF1 is less ordered. This led to four orders of magnitude higher n-channel FET mobility for TI-BDF2 (7×10^{-2} $cm^2V^{-1}s^{-1}$) compared to that of TI-BDF1 ($\sim10^{-6}$ $cm^2V^{-1}s^{-1}$). These two new n-type LC molecules show the effects of molecular structure and side-chain modifications on modulating the LC phase behaviors to result in significantly improved charge-transporting properties. Moreover, mild n-doping of TI-BDF2 could be achieved in

solution-processed thin films by blending with commonly available tetrabutyl phosphonium bromide (TBPB) salt to achieve a high conductivity of 0.40 S cm^{-1}.

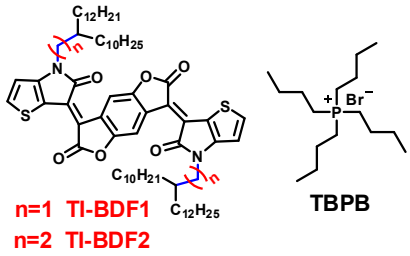

Scheme 1. The structures of TI-BDF1, TI-BDF2 and TBPB

Results and discussion

The synthetic procedure for TI-BDFs (See supporting information) starts from the preparation of N-alkyl-3-thiophenamine via an Ullmann reaction using 3-bromo-thiophene and alkyl amine, follows by cyclizing N-alkyl-3-thiophenamine with oxalyl chloride. Finally, two LCs were synthesized by using the Knoevenagel reaction to condense between 4-alkyl-thieno[3,2-*b*]pyrrole-5,6-dione and benzo[1,2-*b*:4,5-*b*']difuran-2,6(3H,7H)-dione. The structures of the intermediates and two LCs were verified by ^{1}H-NMR, ^{13}C-NMR, and ESI mass spectra (SI).

The results from density function theory (DFT) calculations suggest that these molecules possess coplanar geometry with a very small dihedral angle of less than 0.1° (between thienopyrroledione and benzodifurandione moieties) (**Figure 1c-e**). Such planner structure facilitates molecular stacking and charge delocalization to enhance charge-transporting properties.

As shown in **Figure 1(a)** and **Table 1**, TI-BDF1 and TI-BDF2 show similar absorption spectra with a maximum absorption peak at 656 nm in dilute chloroform solution and a molar extinction coefficient of ~3.77 × 10^4 L mol^{-1} cm^{-1}. Despite the comparable spectra obtained in solution, the thin film absorption spectra are distinctly different from each other. The maximum absorption peak of the TI-BDF1 film is 629 nm (compared to 656 nm in solution) with a weak shoulder peak appears around 720 nm. On the contrary, the absorption peak of TI-BDF2 film is red-shifted to 770 nm (over 100 nm shift) likely due to the formation of tightly packed aggregates.

Noting that, even with only a single carbon difference in side-chain branch point, the two LC molecules exhibit dramatically different solid-state properties. This offers a unique model to study the correlations between molecular structure, phase behavior, and charge transport of molecular semiconductors. Prior to this, we have characterized their basic material properties. The optical band-gaps estimated from the thin film absorption band edge are 1.55 eV (TI-BDF1) and 1.51 eV (TI-BDF2), respectively. The LUMO levels of TI-BDF1 and TI-BDF2 are determined to be −3.88 eV and −3.87 eV, according to the results from cyclic voltammetry (CV) measurements of their thin films (**Figure 1 (b)**). The HOMO levels were estimated to be −5.43 eV (TI-BDF1) and −5.38 eV (TI-BDF2), respectively by subtracting the optical band gaps from the LUMO levels.

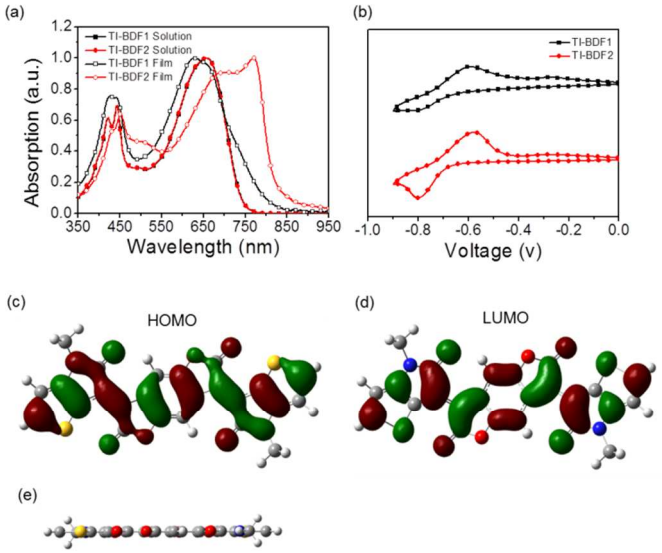

Figure 1. (a) Solution and thin film UV-vis absorption spectra for TI-BDFs. (b) Thin film cyclic voltammograms. Frontier molecular orbitals of (c) the HOMO and (d) LUMO of molecule calculated with DFT. (e) The side view of the optimized molecular structure.

Table 1. Optical and electrochemical properties of the two TI-BDF liquid crystals

LC	Solution		Film		E_g^{opt}	LUMO	HOMO
	λ_{max} [a] (nm)	ε (L mol^{-1} cm^{-1})	λ_{max} (nm)	λ_{edge} (nm)	(eV)	(eV)	(eV)
TI-BDF1	656	3.77 × 10^4	629	800	1.55 [b]	-3.84	-5.39
TI-BDF2	656	3.47 × 10^4	770	820	1.51 [b]	-3.82	-5.33

[a]Measured in chloroform solution.
[b]Band gap estimated from the optical absorption band edge of the films.

The thermotropic LC properties of these two molecules were characterized through differential scanning calorimetry (DSC), polarized optical microscope (POM), and X-ray scattering (XRD) measurements (**Figure 2**). From DSC, TI-BDF1 shows a crystal to LC transition at 50 °C (T_{cr}) and a LC to isotropic transition at ~106 °C (T_{iso}). TI-BDF2 shifts the T_{cr} to a lower temperature at 11 °C and elevates the T_{iso} to 151 °C and it exhibits a wider LC phase window than that of TI-BDF1 (**Figure 2a**). Such phase transition temperature changes indicate that these two molecules have distinctly different phase order and liquid crystallinity due to different branch points on the side-chains. We note that such phase behavior changes were rarely noted in previous thermotropic LC studies. The corresponding phase transition enthalpy of TI-BDF2 at T_{cr} (9.06 KJ/mol) and T_{iso} (28.2 KJ/mol) is also larger than that of TI-BDF1 (T_{cr} = 1.98 KJ/mol and T_{iso} = 10.2 KJ/mol), which suggests that TI-BDF2 could adopt a more ordered LC phase with stronger molecular stacking in solid-state. [23, 33-34]

To better understand their liquid crystalline properties, two LCs show the birefringent features under the polarized optical microscope (POM). A typical fan-type texture for TI-BDF2 was observed (**Figure 2b**) upon cooling from the isotropic phase to 64 °C, indicating a possible smectic liquid crystalline phase.[35-36] The wide angle X-ray diffraction (WAXRD) of TI-BDF2 clearly shows 100, 200 and 300 peaks at 2θ of 3.51, 7.04 and 10.57°, corresponding to a lamellar distance between aromatic segments of 25.2 Å (**Figure S1**). The TI-BDF1 shows

a decreased liquid crystallinity to that of TI-BDF 2 by judging from the combined DSC, POM and WAXRD measurements. The thin film samples of these two molecules annealed at different temperatures have also been subjected to optical orientation studies at room temperature (**Figure S2**). In general, the TI-BDF1 films are less ordered compared to those of TI-BDF2 under varied temperatures, which is consistent with the observed diffused halo peak (**Figure S1**).

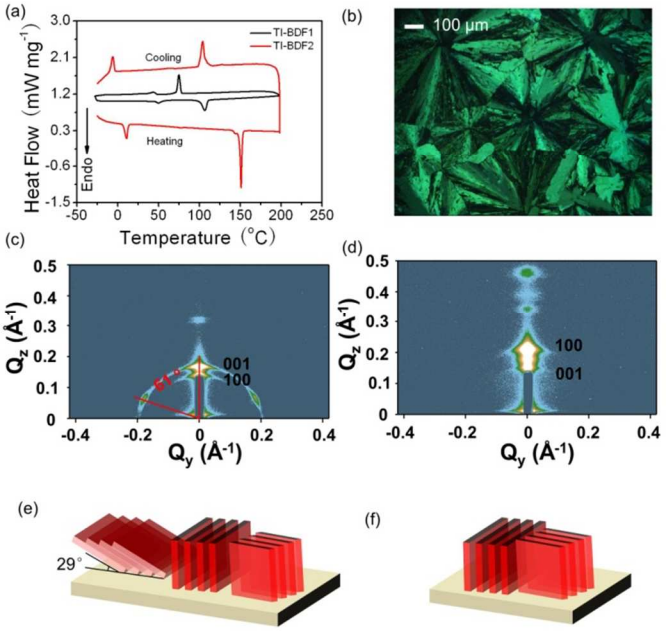

Figure 2. Liquid crystal characterization. (a) The second DSC curves of TI-BDF1 and TI-BDF2 with heating/cooling rates of 10 °C/min. (b) The polarized optical microscopy (POM) image of TI-BDF2 at 64 °C prepared by cooling from isotropic state. 2D GIWAXS patterns of (c) TI-BDF1 film and (d) TI-BDF2 film. The schematic illustration of molecular packing and orientation on silicon substrate for (e) TI-BDF1 and (f) TI-BDF2.

In order to probe the effects of side-chains on the molecular orientation and packing, we have also investigated the annealed films using grazing-incidence wide-angle X-ray scattering (GIWAXS). As shown in **Figure 2c**, the TI-BDF1 film annealed at 80 °C (crystalline state at room temperature) shows a strong diffraction peak at Q = 0.181 Å^{-1} and at Q = 0.210 Å^{-1}, corresponding to a lamellar distance of 34 Å and a conjugated segment length of 30 Å. The integer spacing in these peaks confirms that this feature is coming from the in-plane oriented lamellae in the film. The second Bragg reflection has a preferential alignment at a 61° angle relative to the Q_z axis, and a distinct d-spacing from the first ordered lamellar feature. This suggests that a distinct packing where the lamellar features form domains whose lamellae are out-of-plane with the substrate (**Figure 2e**). In contrast, the TI-BDF2 film annealed at 110 °C (liquid crystalline state at room temperature) only shows a strong in-plane diffraction peak at Q = 0.252 Å^{-1} and a peak at Q = 0.196 Å^{-1}, corresponding to a lamellar distance of 25 Å and a conjugated segment length of 31 Å, respectively (**Figure 2d**). Higher order reflections for both of these features are clearly visible and these features can be therefore assigned to lamellar side-chain packing (**Figure 2f**).

Interestingly, TI-BDF2 shows a smaller lamellar distance than TI-BDF1 though the former possesses a longer side-chain, which indicates that the side-chains on TI-BDF2 may have some degree of inter-digitation. In organic semiconductors, it is well known that edge-on packing of the π-π domains is advantageous for achieving high performance OFETs, due to better charge transport along the horizontally packed backbone; whereas the face-on packing of the π-π domains is considered to be undesirable to impede OFET performance.[37] Based on the GIWAXS results, TI-BDF1 appears to possess two different packing behaviors and molecular orientations. However, it is clear that TI-BDF2 side-chains are strongly aligned in-plane within the film leading to edge-on packing for the π-π domains that would favor high charge mobility.

Atomic force microscopy (AFM) (**Figure 3**) was performed to characterize the top surfaces of the films. The sample films are prepared on BCB/Si substrate using the same procedure for OFET fabrication, and the films were subsequently annealed at a temperature just below T_{iso} (80 °C for TI-BDF1 and 110 °C for TI-BDF2) for 30 min in order to develop ordered LC phase. The TI-BDF1 film shows a relatively small root mean square (RMS) roughness of 1.1 nm (**Figure 3a&c**). However, the TI-BDF2 film has coarse surface with a RMS value of 4.5 nm with grain features indicating high degree of liquid crystallinity (consistent with POM and WAXRD results).

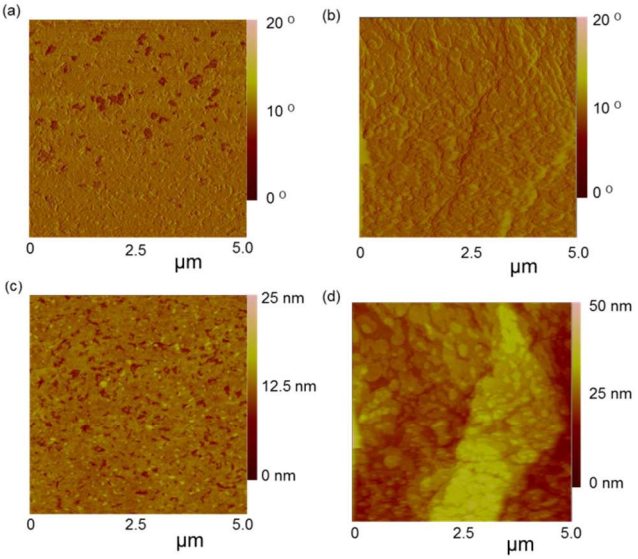

Figure 3. (a) AFM phase image of TI-BDF1 and (b) TI-BDF2 film. (c) AFM height image of TI-BDF1 and (d) TI-BDF2 film.

The charge-transporting properties of two LCs were investigated using a bottom-gate/top-contact FET configuration (**Figure 4a**). A thermally-crosslinked divinyltetramethylsiloxane-bis(benzocyclobutene) (BCB) layer (SI) was spun on silicon oxide dielectric to passivate the surface hydroxyl groups.[38] It is not suprising that the TI-BDF1-based OFET device shows very poor transfer characteristics, and its electron mobility and on–off current ratio is less than 4 × 10^{-6} cm^2 V^{-1} s^{-1} and 50 (**Table 2**), respectively. On the contrary, the TI-BDF2-based device exhibits a typical n-type semiconducting behavior with an on–off current ratio over 2.3×10^6 and an electron mobility (μ_e) of 0.07 cm^2 V^{-1} s^{-1} (**Figure 4c** and **Table 2**), which is almost four orders of magnitude higher than that obtained from TI-BDF 1, while the output characteristics of the device also shows a gate-voltage dependent current (**Figure 4e**). These results correlate well with the observation that TI-BDF2 forms preferable edge-on orientation on substrate and more ordered packing in LC film.

It is also interesting to note that the TI-BDF2 film shows a mobility of 0.04 cm^{2}V^{-1}s^{-1} without annealing after spin-coating

(**Figure S3**), which is comparable to that obtained from being annealed at 110 °C (0.07 $cm^2V^{-1}s^{-1}$). This correlates well with the constant LC phase observed from TI-BDF2 between 11 °C and 151 °C. It is advantageous to achieve high mobility from room temperature processed LCs, compared to commonly observed crystalline materials that need long time and high temperature annealing to achieve high charge mobilities.

Table 2 OFET properties of two liquid crystals

Materials	Mobility	On/off
	$cm^2\ V^{-1}\ s^{-1}$	ratio
TI-BDF1	4×10^{-6}	50
TI-BDF2	7×10^{-2}	2.3×10^6

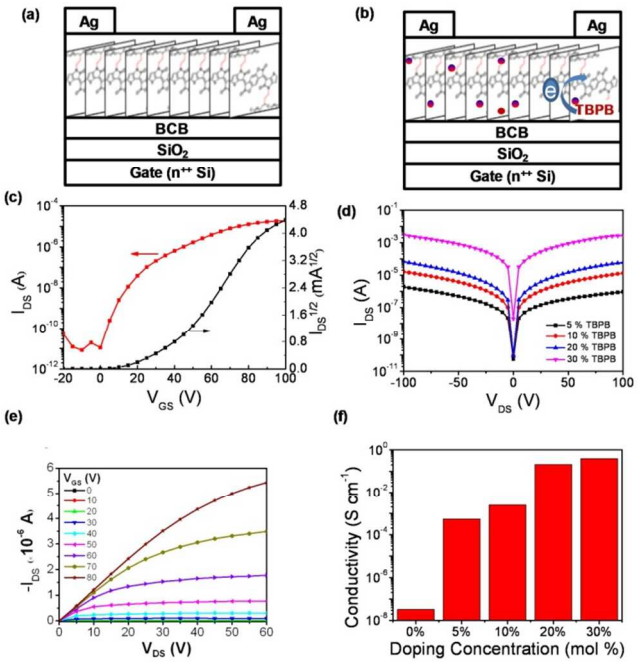

Figure 4. (a-b) Schematic illustration of FET devices. (c) Transfer curves (under V_{DS} = 60 V) and (e) output curves of TI-BDF2 film annealed at 110 °C for 30 minutes. (d) Output curves (under 0 V gate voltage) and (f) conductivity of TBPB-doped TI-BDF2 (without annealing) at varied TBPB concentration.

Solution processable n-doped systems allow improvements in carrier densities and conductivities of n-type semiconductors for applications in organic electronics.[27-28, 39-40] In our previous work, organic ammonium salts have been blended with fullerene derivatives to achieve significantly improved conductivities (~7 orders of magnitude higher than that derived from pure fullerene film). This was attributed to the AIET from the anion of the organic salts to the LUMO of PCBM. We note that the TI-BDF2 and PCBM possess similar LUMO levels, which is energetically favorable for the anion doping process. In this study, a thermally stable phosphonium salt, TBPB was chosen as dopant to improve the conductivity of TI-BDF2 (the device structure shown in **Figure 4b**).

The transfer curves of the device without doping show typical n-type semiconducting characteristics, and the output curves show strong gate voltage dependence (**Figure 4c&e**). Interestingly, after blending TI-BDF2 with TBPB, the device transitioned from the original semiconducting characteristics (without TBPB) to the open channel characteristics (with TBPB) at zero gate voltage (**Figure 4d**), and the output currents showed minimal dependence on the gate-field (**Figure S4**). The conductivity of thin films with varied dopant concentrations are shown in **Figure 4f**. The conductivity of the blend films increased upon the increase of the TBPB concentration, from 3.3×10^{-8} S cm^{-1} (in pristine TI-BDF2) to 5.4×10^{-4} S cm^{-1} (5 mol% TBPB), 2.4×10^{-3} S cm^{-1} (10 mol% TBPB), and 2.1×10^{-1} S cm^{-1} (20 mol% TBPB), respectively. The highest conductivity (0.40 S cm^{-1}) was obtained at a 30% TBPB-doping concentration, which is about 70 times higher than that of the best TBAI-doped PCBM.[28, 41] These results indicate that TBPB-doped TI-BDF2 significantly increased the carrier densities in film upon increasing TBPB ratio and eventually became conducting. TI-BDF2 with LC amorphous grease can be advantageous for doping to accommodate 30 mol% of TBPB without affecting molecular packing during doping to show the highest conductivity (though coarser surface morphology was observed in **Figure 5S**).

Conclusions

In summary, two new n-type LCs have been developed to study their structure/property correlations and to sort out how a minimal molecular strcuture change can be used to affect the macroscopic LC phase and ordering of these LCs for opmizing their charge-transproting proeprties. By extending one more carbon atom on the branching point of the side-chains, coplanar TI-BDFs with distincally different LC phase order and molecular orientation on substrate could be obtained. The highly ordered LC, TI-BDF2, with 3-decylpentadecyl side-chains prefreantially adapts an edge-on π-face orientation with high degree of liquid crystallinity under a broad temperture range, which leads to > 4 orders of magnitude higher electron mobility than that of TI-BDF1 (with 2-decyltetradecyl side-chains). This stable LC property endows room temperature solution-processed TI-BDF2 to have high mobility and conductivity after being doped by a thermally stable phosphonium salt. It showed a very respectable conductivity of 0.40 S cm^{-1} for solution processed n-doping systems.[40] This study not only brings new insights on designing novel n-type semiconductors, but also demonstrates the potential of using solution-processible n-doped organics for wide range of organic electronic applications.

Experimental Section

All chemicals were purchased from Aldrich or VWR International, and used without purification. Benzo[1,2-*b*:4,5-*b*']difuran-2,6(3H,7H)-dione was prepared according to literature procedures.[9] UV-Vis spectra were measured using a Perkin-Elmer Lambda-9 spectrophotometer. The ^1H and ^{13}C NMR spectra were collected on a Bruker AV500 spectrometers operating at 500 and 125 MHz, respectively, in deuterated chloroform solution referenced to TMS. Mass spectrometry data was collected on a Bruker Esquire mass spectrometer using electrospray ionization. Thermal transitions were measured on a TA Instruments Q20–1066 Differential Scanning Calorimeter with a heating rate of 5 °C min^{-1}.

Cyclic voltammetry of the films was conducted in acetonitrile with 0.1 M tetrabutylammonium hexafluorophosphate using a scan rate of 100 mV s^{-1}. An ITO, Ag/AgCl, and Pt mesh were used as the working electrode, reference electrode, and counter electrode, respectively. The wide angle X-ray diffraction pattern was obtained by a Bruker D8 Advance X-Ray diffractometer. The polar optical microscopy image was recorder by a Leica DM 4500 P polarizing microscope, and the optical orientation images was recorded by a video CCD camera (IK-M48PK Toshiba, single-chip color camera) attached to the microscope (Reichert Zetopan) with a camera-

rotating polarizer unit and a circular polarizer.[42] AFM images under tapping mode were taken on a Veeco multimode AFM with a Nanoscope III controller.

Fabrication and characterization of OTFT devices: The field-effect transistors based on two LCs were fabricated using the top-contact and bottom-gate geometry. Heavily doped n-type silicon substrates with a 300 nm thermal oxide layer were purchased from the Montco Silicon Technologies INC. After cleaning the substrate by sequential ultrasonication in acetone and isopropyl alcohol for 15 min followed by air plasma treatment, the oxide layer was passivated with a thin BCB buffer layer. 1 wt% BCB precursor solution in toluene was spun onto the silicon oxide at 4000 rpm and subsequently annealed at 250 °C overnight. The total capacitance density measured from parallel-plate capacitors was 10.6 nF cm^{-2}. The different LC films were spin-coated chloroform solution. The thickness of the films is around 30 nm estimated from AFM measurement, and the blending films were considered as a single-layer for conductivity calculation. Interdigitated source and drain electrodes (W=1000 μm, L= 20 μm) were defined by evaporating a layer of Ag (50 nm) through a shadow mask at 10^{-7} Torr. OFET characterization was carried out in a N_2–filled glovebox using an Agilent 4155B semiconductor parameter S6 analyzer. The field-effect mobility was calculated from the linear fit of $(I_{DS})^{1/2}$ vs V_{GS} in the saturation regime. The threshold voltage (V_t) was estimated as the x intercept of the linear section of the plot of $(I_{DS})^{1/2}$ vs V_{GS}. Conductivities were measured in the N_2 glove box and derived from gated two-terminal measurements at zero gate voltage with the equation of $\sigma = (L/A)(I_{DS}/V_{DS})$, where L (m) and A ($m^2$) are the channel length and cross-sectional area of the devices,[24, 28] respectively.

Acknowledgements

The authors thank the support from the Air Force Office of Scientific Research (No. FA9550-09-1-0426), the Asian Office of Aerospace R&D (No. FA2386-11-1-4072), and the Office of Naval Research (No. N00014-14-1-0170). A. K.-Y. Jen thanks the Boeing Foundation for support. X.S.L. and F.Z.D. acknowledge US NSF (CHE-1265945) for support. Authors thank Dr. Werner Kaminsky for optical orientation characterization.

Notes and references

[a]Department of Materials Science and Engineering, University of Washington, Seattle, WA 98195-2120, USA.
[b]College of Chemistry, Xiangtan University, Xiangtan 411105, PR China.
[c]Department of Chemical Engineering, University of Washington, Seattle, WA 98195, USA.
[d]Department of Chemistry, University of Washington, Seattle, WA, 98195–1700, USA.

†Z.B. and C.-Z. Li contributed equally to this work.
E-mail: ajen@u.washington.edu

Electronic Supplementary Information (ESI) available: synthesis of the chemicals, characterization data. See DOI: 10.1039/b000000x/ Electronic

1. C. Wang, H. Dong, W. Hu, Y. Liu and D. Zhu, *Chem. Rev.*, 2011, **112**, 2208-2267.
2. Y. Zhao, Y. Guo and Y. Liu, *Adv. Mater.*, 2013, **25**, 5372-5391.
3. J. E. Anthony, A. Facchetti, M. Heeney, S. R. Marder and X. Zhan, *Adv. Mater.*, 2010, **22**, 3876-3892.
4. X. Gao and Y. Hu, *J. Mater. Chem. C*, 2014, **2**, 3099-3117.
5. X. Guo, A. Facchetti and T. J. Marks, *Chem. Rev.*, 2014, **114**, 8943-9021.
6. C.-Z. Li, H.-L. Yip and A. K. Y. Jen, *J. Mater. Chem.*, 2012, **22**, 4161-4177.
7. C. Kanimozhi, N. Yaacobi-Gross, K. W. Chou, A. Amassian, T. D. Anthopoulos and S. Patil, *J. Am. Chem. Soc.*, 2012, **134**, 16532-16535.
8. Y. Qiao, Y. Guo, C. Yu, F. Zhang, W. Xu, Y. Liu and D. Zhu, *J. Am. Chem. Soc.*, 2012, **134**, 4084-4087.
9. T. Lei, J. H. Dou, X. Y. Cao, J. Y. Wang and J. Pei, *J. Am. Chem. Soc.*, 2013, **135**, 12168-12171.
10. T. M. Pappenfus, R. J. Chesterfield, C. D. Frisbie, K. R. Mann, J. Casado, J. D. Raff and L. L. Miller, *J. Am. Chem. Soc.*, 2002, **124**, 4184-4185.
11. R. S. Ashraf, A. J. Kronemeijer, D. I. James, H. Sirringhaus and I. McCulloch, *Chem. Commun.*, 2012, **48**, 3939-3941.
12. T. Lei, J.-Y. Wang and J. Pei, *Acc. Chem. Res.*, 2014, **47**, 1117-1126.
13. F. Zhang, Y. Hu, T. Schuettfort, C. A. Di, X. Gao, C. R. McNeill, L. Thomsen, S. C. Mannsfeld, W. Yuan, H. Sirringhaus and D. Zhu, *J. Am. Chem. Soc.*, 2013, **135**, 2338-2349.
14. T. Lei, J. H. Dou and J. Pei, *Adv. Mater.*, 2012, **24**, 6457-6461.
15. J. Lee, A. R. Han, H. Yu, T. J. Shin, C. Yang and J. H. Oh, *J. Am. Chem. Soc.*, 2013, **135**, 9540-9547.
16. E. M. Garcia-Frutos, U. K. Pandey, R. Termine, A. Omenat, J. Barbera, J. L. Serrano, A. Golemme and B. Gomez-Lor, *Angew. Chem. Int. Ed*, 2011, **50**, 7399-7402.
17. C.-Z. Li, Y. Matsuo and E. Nakamura, *J. Am. Chem. Soc.*, 2009, **131**, 17058-17059.
18. C.-Z. Li, Y. Matsuo and E. Nakamura, *J. Am. Chem. Soc.*, 2010, **132**, 15514-15515.
19. M. Funahashi and J. I. Hanna, *Adv. Mater.*, 2005, **17**, 594-598.
20. M. O'Neill and S. M. Kelly, *Adv. Mater.*, 2003, **15**, 1135-1146.
21. K. Isoda, T. Abe, M. Funahashi and M. Tadokoro, *Chem. Eur. J.*, 2014, **20**, 7232-7235.
22. H. Iino and J. I. Hanna, *J. Phys. Chem. B*, 2005, **109**, 22120-22125.
23. M.-A. Muth, M. Carrasco-Orozco and M. Thelakkat, *Adv. Funct. Mater.*, 2011, **21**, 4510-4518.
24. P. Wei, J. H. Oh, G. Dong and Z. Bao, *J. Am. Chem. Soc.*, 2010, **132**, 8852-8853.
25. S. Guo, S. B. Kim, S. K. Mohapatra, Y. Qi, T. Sajoto, A. Kahn, S. R. Marder and S. Barlow, *Adv. Mater.*, 2012, **24**, 699-703.
26. B. D. Naab, S. Guo, S. Olthof, E. G. B. Evans, P. Wei, G. L. Millhauser, A. Kahn, S. Barlow, S. R. Marder and Z. Bao, *J. Am. Chem. Soc.*, 2013, **135**, 15018-15025.
27. B. A. Gregg and R. A. Cormier, *J. Am. Chem. Soc.*, 2001, **123**, 7959-7960.
28. C.-Z. Li, C.-C. Chueh, H.-L. Yip, F. Ding, X. Li and A. K. Y. Jen, *Adv. Mater.*, 2013, **25**, 2457-2461.
29. D. Sun, S. V. Rosokha and J. K. Kochi, *J. Phys. Chem. B*, 2007, **111**, 6655-6666.
30. S. Guha, F. S. Goodson, L. J. Corson and S. Saha, *J. Am. Chem. Soc.*, 2012, **134**, 13679-13691.
31. R. E. Dawson, A. Hennig, D. P. Weimann, D. Emery, V. Ravikumar, J. Montenegro, T. Takeuchi, S. Gabutti, M. Mayor, J. Mareda, C. A. Schalley and S. Matile, *Nat. Chem.*, 2010, **2**, 533-538.
32. K. M. O'Malley, C.-Z. Li, H.-L. Yip and A. K. Y. Jen, *Adv. Energy Mater.*, 2012, **2**, 82-86.
33. S.-Y. Park, T. Zhang, L. V. Interrante and B. L. Farmer, *Macromolecules*, 2002, **35**, 2776-2783.
34. R. Yang, L. Chen, C. Ruan, H.-Y. Zhong and Y.-Z. Wang, *Journal of Materials Chemistry C*, 2014, **2**, 6155-6164.
35. B. Zhao, B. Liu, R. Q. Png, K. Zhang, K. A. Lim, J. Luo, J. Shao, P. K. H. Ho, C. Chi and J. Wu, *Chem. Mater.*, 2010, **22**, 435-449.
36. H. Fujikake, T. Murashige, M. Sugibayashi and K. Ohta, *Appl. Phys. Lett.*, 2004, **85**, 3474-3476.
37. H. Sirringhaus, P. J. Brown, R. H. Friend, M. M. Nielsen, K. Bechgaard, B. M. W. Langeveld-Voss, A. J. H. Spiering, R. A. J. Janssen, E. W. Meijer, P. Herwig and D. M. de Leeuw, *Nature*, 1999, **401**, 685-688.
38. L. L. Chua, J. Zaumseil, J. F. Chang, E. C. W. Ou, P. K. H. Ho, H. Sirringhaus and R. H. Friend, *Nature*, 2005, **434**, 194-199.

39. R. A. Schlitz, F. G. Brunetti, A. M. Glaudell, P. L. Miller, M. A. Brady, C. J. Takacs, C. J. Hawker and M. L. Chabinyc, *Adv. Mater.*, 2014, **26**, 2825-2830.
40. B. D. Naab, S. Zhang, K. Vandewal, A. Salleo, S. Barlow, S. R. Marder and Z. Bao, *Adv. Mater.*, 2014, **26**, 4268-4272.
41. C.-Z. Li, C.-C. Chueh, F. Ding, H.-L. Yip, P.-W. Liang, X. Li and A. K. Y. Jen, *Adv. Mater.*, 2013, **25**, 4425-4430.
42. W. Kaminsky, E. Gunn, R. Sours and B. Kahr, *J Microsc-Oxford*, 2007, **228**, 153-164.